Analyst

ROYAL SOCIETY OF CHEMISTRY

PAPER

View Article Online
View Journal | View Issue

Cite this: *Analyst*, 2023, **148**, 6341

Quantitative analysis of SO_2, NO_2 and NO mixed gases based on ultraviolet absorption spectrum

Yibiao Yang, [a,b] Jinhuan Li,[c] Zihui Zhang,*[a] Jianing Wang*[a] and Guanyu Lin[a]

Received 21st August 2023,
Accepted 30th October 2023

DOI: 10.1039/d3an01431b

rsc.li/analyst

SO_2, NO_2 and NO are the main atmospheric pollutants produced by the combustion of fossil fuel. Detecting these gases is of great significance for atmospheric protection and the online concentration detection of pollutants. In this study, the concentration retrieval methods of NO, NO_2 and SO_2 and their mutual effects were studied in the wavelength range of 192.3–254.4 nm. In this band, NO, NO_2 and SO_2 have large absorption cross-sections; however, their spectrum superpositions were serious. A novel method was proposed to separate the superposed absorption spectra of NO and SO_2 or NO_2. The advantage of this method is that it can remove the influence of SO_2 and NO_2 on NO concentration retrieval. The fast Fourier transform (FFT) amplitude method was used to calculate the concentrations of SO_2 and NO_2, and the direct absorption spectroscopy method was used to calculate NO concentration. *Via* these methods, the gas concentrations of SO_2, NO_2 and NO can be calculated in ternary-gas mixtures. The experimental results show that these methods can effectively remove the mutual interferences between the concentration retrieval of NO, NO_2 and SO_2. The maximum absolute values of the relative deviations for the concentration retrieval of SO_2, NO_2 and NO in ternary-gas mixtures are 3.868%, 4.740% and 5.008%, respectively. These methods have high detection precision and good adaptability and are suitable for online flue detection equipment.

1. Introduction

Sulfur dioxide (SO_2) is one of the main atmospheric pollutants produced by fossil fuel combustion and volcanic eruption.[1,2] When the SO_2 concentration in the surrounding environment exceeds 0.21 ppm, it can harm human health, such as causing respiratory diseases.[2,3] The SO_2 in the air returns to the ground with rainwater, thereby corroding buildings and equipment and damaging water and forest ecosystems.[1,4] Nitrogen oxides (NO_X, which mainly includes NO and NO_2) mainly come from the combustion of fossil fuel and biomass, lightning and microbial activity.[5] The NO_X in the air can combine with water, ammonia, and other organic gases to form smog and acid rain, damaging the ecological environment.[2,6,7] With the rapid development of economy, the use of fossil fuel is increasing to generate power to meet the energy needs of human activities. This will cause an increase in SO_2 and NO_x emissions and further exacerbate environmental pollution. In order to ensure a healthy living environment and achieve sustainable development of human beings, the Chinese government has issued regulations requiring the concentrations of SO_2 and NO_X emitted by thermal power plants to be lower than 35 ppm and 48.7 ppm, respectively.[8] Because detecting pollutant gas concentrations is an essential prerequisite for controlling emissions, it is of great significance to study methods for detecting SO_2 and NO_x concentrations.

At present, the main methods for gas detection include the metal oxide sensor method and optical methods.[9] Metal oxide sensors are widely applied in detecting the concentrations of SO_2 and NO due to their low cost. However, the performance of metal oxide sensors deteriorates with increasing working hours and is susceptible to temperature and humidity changes.[9,10] Although some metal oxide sensors can operate at room temperature, their poor stability and repeatability limit their widespread application in the field of high-precision and real-time detection.[9] Optical methods mainly include photoacoustic spectroscopy (PAS), tunable diode laser absorption spectroscopy (TDLAS), non-dispersive infrared spectroscopy (NDIR), differential optical absorption spectroscopy (DOAS), *etc*.[11] Due to the good collimation of lasers, TDLAS easily achieves a considerable optical path, so it can achieve high-precision detection. However, the equipment for TDLAS is relatively expensive and can only detect one kind of gas at a time with poor scalability.[12,13] NDIR uses infrared light as the detection system's light source. It can detect NO_2 and NO in a large concentration range, but is susceptible to interference from

[a]*Changchun Institute of Optics, Fine Mechanics and Physics, Chinese Academy of Sciences, Changchun 130033, China. E-mail: zhangzihui123@126.com, qazedcfv@sina.com*
[b]*University of Chinese Academy of Sciences, Beijing 100049, China*
[c]*Shanghai Institute of Satellite Engineering, Shanghai 201100, China*

water vapor and has poor anti-interference ability and large measurement deviations.[14] Moreover, when measuring multiple gases, it requires multiple measurement channels, increasing hardware costs.[13,14] DOAS has good scalability, high selectivity, high economy, and high accuracy and can simultaneously detect multiple gases. Therefore, it has been widely applied in the field of multiple gas detection.[5,14] However, DOAS also faces the following challenge: under extremely low concentration conditions, the spectral signal received by the traditional detection systems is easily affected by noise, making it difficult to achieve high-precision detection.[14,15]

There are two main solutions to the current problem of using DOAS technology to detect gas concentrations: the first method is to use an absorption cell with a long optical path to improve the signal-to-noise ratio of the detection system, as shown in ref. 2; the second method is to select the gas absorption band with the larger absorption cross-section as the gas retrieval wavelength band. However, deuterium lamps, which are often used as the light source in the DOAS detection systems, have a large divergence angle and are difficult to achieve good collimation like lasers, making it difficult to achieve a long optical path in detection systems. NO, SO_2 and NO_2 have large absorption cross-sections in the wavelength range of 192–255 nm, but their absorption cross-sections are mixed with each other, as shown in Fig. 1,[16] bringing difficulties to gas concentration retrieval. In the field of low concentration and high-precision mixed gas detection, research on separation methods for superposed absorption spectra has great application potential. For example, ref. 14 studied the absorption spectra of mixtures of SO_2 and NO and achieved SO_2 measurement deviations from −4% to 1.19%.

In this paper, DOAS and direct absorption spectroscopy are used to separate the superposed absorption spectra of NO_2, SO_2 and NO mixed gases in the wavelength range of 192.3–254.4 nm. This method makes full use of the advantage of the large absorption cross-section in this wavelength range to improve the concentration retrieval precision of the gases in SO_2, NO_2 and NO mixtures.

2. Theory

2.1 Lambert–Beer law

The propagation of a monochromatic beam with wavelength λ in a specific gas is expressed by the Lambert–Beer law[2,10,17,18] as shown in eqn (1), where $I_0(\lambda)$ is the light intensity of the monochromatic beam with wavelength λ which isn't absorbed by the gas to be measured, $I(\lambda)$ is the remaining light intensity after being absorbed by the gas, $\sigma(\lambda)$ is the absorption cross-section of the gas to be measured at wavelength λ (cm^2 per molecule), L is the optical path of the beam propagating in the gas (cm) and C is the gas concentration (molecule per cm^3).

$$I(\lambda) = I_0(\lambda) \times \exp[-\sigma(\lambda)CL] \quad (1)$$

The Rayleigh scattering $\varepsilon_R(\lambda)$ and Mie scattering $\varepsilon_M(\lambda)$ of the gas molecules also play a role in reducing the light intensity of the beam propagating in the gas, so eqn (1) can be revised as eqn (2). The meanings of the other parameters in eqn (2) are the same as in eqn (1).

$$I(\lambda) = I_0(\lambda) \times \exp[-\sigma(\lambda)CL - \varepsilon_R(\lambda) - \varepsilon_M(\lambda)] \quad (2)$$

Because nitrogen is hardly absorbed in the wavelength range of 192.3–254.4 nm, there is only Rayleigh scattering and Mie scattering. Therefore, the Rayleigh scattering and Mie scattering in eqn (2) can be replaced by measuring high-purity nitrogen, as shown in eqn (3). In eqn (3), $I'_0(\lambda)$ is the light intensity when the gas to be measured is high-purity nitrogen, and the meanings of the other parameters are the same as in eqn (2).

$$I'_0(\lambda) = I_0(\lambda) \times \exp[-\varepsilon_R(\lambda) - \varepsilon_M(\lambda)] \quad (3)$$

Substituting eqn (3) into eqn (2), the result is eqn (4). Taking the logarithm of eqn (4), the result is eqn (5). $A(\lambda)$ is the gas absorbance in eqn (5). According to eqn (5), there is a linear relationship between the concentration of a specific gas

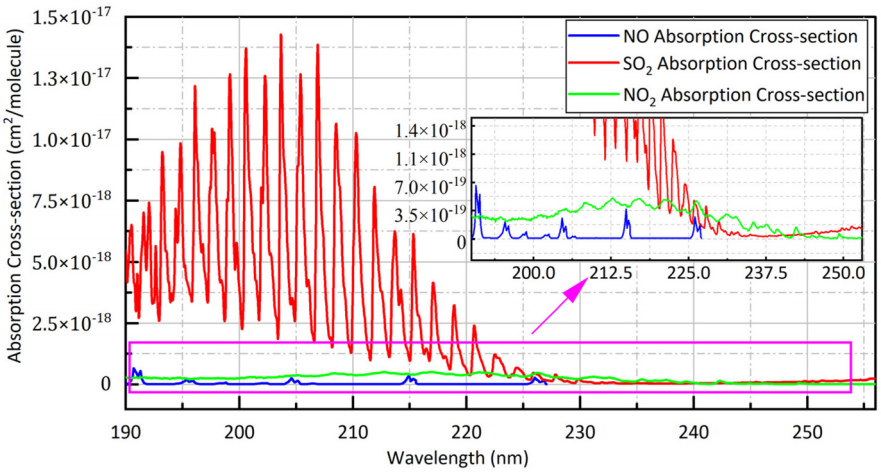

Fig. 1 Absorption cross-sections of NO, NO_2 and SO_2 at 190–256 nm.[16,24]

and its absorbance, which is the theoretical basis for gas measurement based on the absorption spectroscopy method.[18]

$$I(\lambda) = I'_0(\lambda) \times \exp[-\sigma(\lambda)CL] \quad (4)$$

$$A(\lambda) = \ln\left(\frac{I'_0(\lambda)}{I(\lambda)}\right) = \sigma(\lambda)CL \quad (5)$$

2.2 Differential optical absorption spectroscopy

In the DOAS theory, a gas absorption cross-section can be divided into two parts, as shown in eqn (6): one part is the slow-varying part which varies slowly with wavelength, and the other is the fast-varying part which varies rapidly with the wavelength. In eqn (6), $\sigma^f(\lambda)$ and $\sigma^s(\lambda)$ are the fast-varying part and the slow-varying part respectively, and the meanings of the other parameters are the same as in eqn (2).[2,19,20]

$$I(\lambda) = I_0(\lambda) \times \exp[-(\sigma^f(\lambda) + \sigma^s(\lambda))CL - \varepsilon_R(\lambda) - \varepsilon_M(\lambda)] \quad (6)$$

Just like in the previous section, the Rayleigh scattering and Mie scattering in eqn (6) are replaced by measuring high-purity nitrogen. Taking the logarithm of eqn (6), the result is shown as eqn (7). In eqn (7), $A'(\lambda)$ is the absorbance of the gas to be measured. As shown in eqn (8), the fast-varying part can represent the concentration information of the gas, and DOD (λ) is the differential absorbance of the gas. It is known from eqn (8) that the DOD(λ) of a specific gas is linearly related to the gas concentration. Therefore, DOD(λ) can be used to retrieve the gas concentration.

$$A'(\lambda) = \ln\left(\frac{I'_0(\lambda)}{I(\lambda)}\right) = \left(\sigma^f(\lambda) + \sigma^s(\lambda)\right)CL \quad (7)$$

$$\mathrm{DOD}(\lambda) = \sigma^f(\lambda)CL \quad (8)$$

However, when using eqn (8) for gas measurement, the gas to be measured must be a single component gas and eqn (8) cannot be used when the gas to be measured is a mixture of multiple gases. When measuring mixtures of multiple gases, eqn (6) is adjusted to eqn (9),[2,21,22] where $\sigma_i^f(\lambda)$ and $\sigma_i^s(\lambda)$ are the fast-varying part and the slow-varying part, respectively, of the absorption cross-section of the i-th gas. The meanings of the other parameters in eqn (9) are the same as in eqn (6).

$$I(\lambda) = I_0(\lambda) \times \exp\left[-\sum_{i=1}^{n}\left(\sigma_i^f(\lambda) + \sigma_i^s(\lambda)\right)C_iL - \varepsilon_R(\lambda) - \varepsilon_M(\lambda)\right] \quad (9)$$

Just like in the measurement of a single gas, the Rayleigh scattering and Mie scattering in eqn (9) are replaced by measuring high-purity nitrogen and then taking the logarithm of eqn (9). The result is shown as eqn (10), where $A''(\lambda)$ is the absorbance of the multiple gases. Using a mathematical method to filter out the slow-varying parts of multiple gases, the differential absorbance of multiple gases can be obtained, as shown in eqn (11).[1,14]

$$A''(\lambda) = \ln\left(\frac{I'_0(\lambda)}{I(\lambda)}\right) = \sum_{i=1}^{n}\left(\sigma_i^f(\lambda) + \sigma_i^s(\lambda)\right)C_iL \quad (10)$$

$$\mathrm{DOD}'(\lambda) = \sum_{i=1}^{n}\sigma_i^f(\lambda)C_iL \quad (11)$$

When using DOAS to measure multiple gases, it is necessary to filter out the slow-varying parts of different gases and obtain a differential absorbance that can represent the concentration information of multiple gases. However, the slow-varying parts of different gases have different characteristics, making it difficult to find a suitable method to simultaneously filter out the slow-varying part of different gases.

3. Experimental system setup

The schematic diagram of the measurement system is shown in Fig. 2. A deuterium lamp (Hamamatsu L6301, Japan) which has a strong and continuous emission spectrum in the ultraviolet band is used as the light source of the measurement system. The broad band ultraviolet light emitted by the deuterium lamp is coupled into an anti-ultraviolet (anti-UV) optical fiber whose numerical aperture is 0.22, and the outgoing light of the anti-UV optical fiber is collimated by a parabolic reflector (Thorlabs MPD01M9-F01, USA) and then enters a gas absorption cell. The optical path of the absorption cell is 700 mm.

When the ultraviolet light passes through the gas absorption cell with fused silica window glass, the photons of a specific wave band are absorbed by the gas to be measured. The parabolic reflector and the fused silica window glass absorb little in the ultraviolet band. Photons that aren't absorbed by the gas are focused by another parabolic reflector (Thorlabs MPD01M9-F01, USA) and then coupled into another anti-UV optical fiber. The output end of the optical fiber is connected to an ultraviolet spectrometer (GanWei GW-5040, China) which works in the wavelength range of 180–400 nm with a sampling interval of 0.1 nm.

The gases used in the experiment are from Dalian Special Gases Co., Ltd. The uncertainties of SO_2, NO_2 and NO are all 2%. The gases in the cylinders pass through pressure reducing

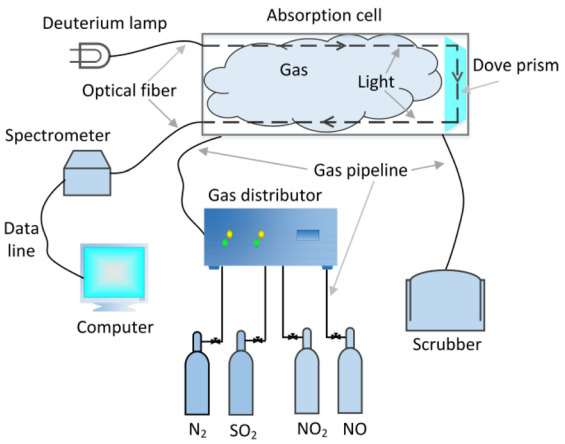

Fig. 2 Schematic diagram of measurement system.[24]

valves and then flow along a gas pipeline to a gas distribution instrument (SWISSGAS Sonimix7100, Switzerland) with an accuracy error of 0.5%. The gas mixed by the gas distributor enters the gas absorption cell. The measured gas is discharged into the atmosphere after tail gas treatment.

The whole experimental process was conducted at room temperature and atmospheric pressure, and the influence of temperature and pressure on the experimental results was relatively small and could be ignored.[1,14]

At the beginning of the experiment, the experimental equipment was turned on to preheat for 30 minutes, and the pressure reducing valves were adjusted to maintain 0.3–0.5 MPa, meeting the input pressure requirement of the gas distributor. During the whole measurement process, the flow rate of the gas flowing into the absorption cell remained unchanged at 350 ml min^{-1}.

Then, nitrogen flowed into the gas absorption cell at a flow rate of 350 ml min^{-1} for 200 s to ensure that the absorption cell was completely filled with pure nitrogen. Spectral data were collected with the ultraviolet spectrometer. The integration time of the spectrometer was 19 ms to ensure that the spectral signal had a high signal-to-noise ratio and didn't exceed the maximum code value of the spectrometer detector. The spectral signal received at this time by the spectrometer was denoted as $I'_0(\lambda)$. Then, the absorption spectral signals of the mixed gases were collected, and the operation processes of filling the mixed gases were the same as that of filling nitrogen. The spectral signals of the mixed gases were recorded as $I(\lambda)$. 50 groups of spectral data were collected for each measurement.

4. Method and results

4.1 Signal-gas retrieval express

4.1.1 NO. The experiment collected 14 groups of NO gas with concentrations ranging from 42 ppm to 92 ppm. Fig. 3 and 4 show the spectral signals and the absorbances of partial NO concentrations. It can be seen from Fig. 4 that there are obvious absorption peaks for NO at 192.3 nm, 205.5 nm, 215.4 nm, and 226.5 nm. However, the peak value of the NO absorption peak at 192.3 nm was higher than the others.

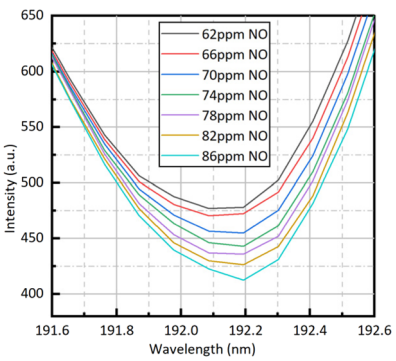

Fig. 3 Absorption spectra of NO with different concentrations.

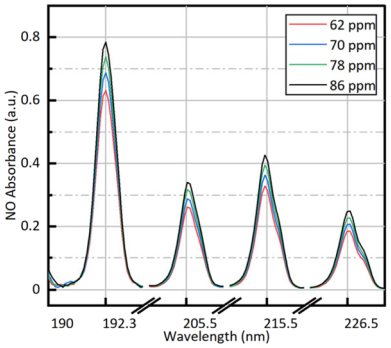

Fig. 4 Absorbance of NO with different concentrations.

Although the deuterium lamp has weak emission intensity at 192.3 nm, the signal-to-noise ratio of its light intensity at 192.3 nm meets the requirement of the gas spectral signal process for signal-to-noise ratio. Since the absorption peaks of NO are discontinuous, the direct absorption spectroscopy method was used to retrieve NO concentrations. The mathematical expression of the direct absorption spectroscopy method is shown in eqn (7). The absorbances at 192.3 nm of different concentrations of NO were fitted with the NO concentrations, and the fitting results are shown in Fig. 5 and eqn (12), where A_{NO} is the NO absorbance at 192.3 nm, and C_{NO} is the retrieval concentration of NO. The goodness of fit between the NO absorbances at 192.3 nm and the NO concentrations reaches 0.9944. According to the fitting results in Fig. 5 and eqn (12), the NO absorbances at 192.3 nm has a good linear relationship with NO concentrations and the high-precision concentration retrieval of NO can be achieved based on the relationship between the NO absorbances at 192.3 nm and the NO concentrations.

$$C_{NO} = 143.269 \times A_{NO} - 27.353 \quad (12)$$

4.1.2 SO_2. As shown in Fig. 1, SO_2 has a large absorption cross-section at 193–225 nm and 275–313 nm, but the SO_2 absorption cross-section at 193–223 nm changes more quickly with wavelength and is larger than that at 275–313 nm.[23] In order to achieve detection under low concentration conditions,

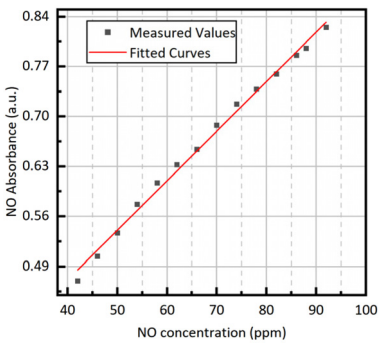

Fig. 5 Relationship between NO concentration and the absorbance at 192.3 nm.

the wavelength range of 193–223 nm with the large SO_2 absorption cross-section is selected as the retrieval wavelength band of SO_2. The experiment collected 20 groups of SO_2 with different concentrations ranging from 26 ppm to 102 ppm. Fig. 6 shows the absorbances of SO_2 at concentrations of 30 ppm, 50 ppm, and 70 ppm. It can be seen from Fig. 6 that the absorbance increases with increasing SO_2 concentration and changes sharply with wavelength. These provide conditions for the concentration retrieval of SO_2 based on the FFT amplitude method. As shown in Fig. 7, the FFT amplitude at 0.628 nm^{-1} of the SO_2 absorbance increases with increasing SO_2 concentration. Therefore, the SO_2 absorbances at 193–223 nm were transformed by FFT and then the FFT amplitudes at 0.628 nm^{-1} were fitted with the SO_2 concentrations.[24] The fitting relationship between the FFT amplitudes at 0.628 nm^{-1} of SO_2 absorbances and the SO_2 concentrations is shown in Fig. 8 and eqn (13) and their goodness of fit reaches 0.9998. In eqn (13), AMP_{SO_2} is the SO_2 FFT amplitude at 0.628 nm^{-1}, and C_{SO_2} is the retrieval concentration of SO_2. From the above analysis, it can be concluded that the FFT amplitude at 0.628 nm^{-1} of SO_2 absorbance can accurately retrieve SO_2 concentration.

$$C_{SO_2} = 573.252 \times AMP_{SO_2} - 27.561 \quad (13)$$

4.1.3 NO_2. In this paper, the wavelength range of 229.1–254.4 nm was selected as the retrieval wavelength band of NO_2. As shown in Fig. 1, although NO_2 has a small absorption cross-section at 229.1–254.4 nm, the absorption cross-section of SO_2 in this band is smaller than that of NO_2, so NO_2 concentration retrieval is less affected by SO_2. Also, at 229.1–254.4 nm, the deuterium lamp is bright, so the absorption spectral signal of NO_2 has a high signal-to-noise ratio. Due to the continuous absorption cross-section of NO_2, the FFT amplitude method was used to retrieve NO_2 concentration. The experiment collected 13 groups of NO_2 with different concentrations ranging from 40 ppm to 88 ppm. Fig. 9 and 10 show the absorbances and FFT amplitudes of

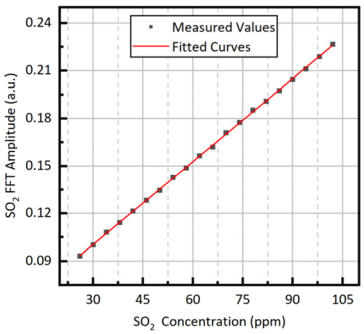

Fig. 8 Relationship between SO_2 concentration and the FFT amplitude at 0.628 nm^{-1}.

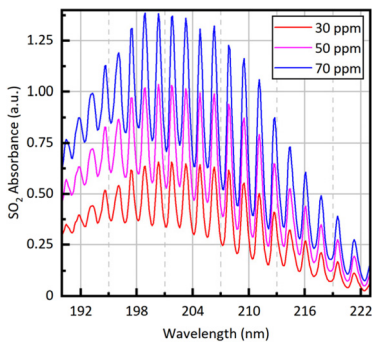

Fig. 6 SO_2 absorbance with different concentrations.

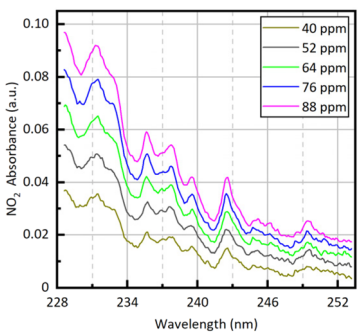

Fig. 9 NO_2 absorbance with different concentrations.

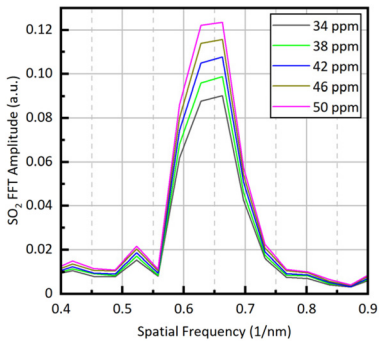

Fig. 7 FFT amplitude of the absorbance at 193–223 nm of SO_2 with different concentrations.

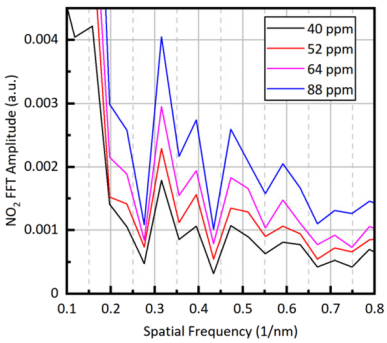

Fig. 10 FFT amplitude of the absorbance at 229.1–254.4 nm of NO_2 with different concentrations.

partial concentrations of NO_2, respectively. It can be seen from Fig. 9 and 10 that the absorbance and FFT amplitude of NO_2 increase with increasing NO_2 concentration. The FFT amplitudes at 0.315 nm^{-1} of NO_2 absorbance were fitted with the NO_2 concentrations; the fitting results are shown in Fig. 11 and eqn (14), and their goodness of fit reaches 0.9963. In eqn (14), AMP_{NO_2} is the NO_2 FFT amplitude at 0.315 nm^{-1}, and C_{NO_2} is the retrieval concentration of NO_2. From the above analysis, it can be seen that the FFT amplitude of NO_2 absorbance can be used for NO_2 concentration retrieval.

$$C_{NO_2} = 20\,022.245 \times AMP_{NO_2} + 5.348 \quad (14)$$

4.2 Binary-gases retrieval express

4.2.1 SO_2 concentration retrieval. In the wavelength range of 193–223 nm, SO_2 has a larger absorption cross-section than NO_2 and NO, so SO_2 is less influenced by NO and NO_2 within the emission concentration range required by the rules. Moreover, in this paper, the FFT amplitude method is used to retrieve SO_2 concentration, which further reduces the influence of NO_2 and NO on the retrieval accuracy of SO_2. Just like single SO_2 concentration retrieval, the FFT amplitude at 0.628 nm^{-1} of the absorbance at 193–223 nm was selected as the eigenvalue for the concentration retrieval of SO_2 mixed with NO_2 or NO.

In order to study the influence of NO_2 on SO_2 concentration retrieval, the spectral data of gas mixtures with different concentrations of SO_2 and NO_2 were collected in the experiment. When the concentrations of SO_2 were 24 ppm and 52 ppm, the concentration range of NO_2 was from 20 ppm to 52 ppm at intervals of 4 ppm. The results of this experiment are shown in Fig. 12. It can be seen from Fig. 12 that, no matter how the concentration of NO_2 changes in the mixed gases of NO_2 and SO_2, there is no significant change in the eigenvalues of SO_2 which represent the concentration information of SO_2. Therefore, in the process of SO_2 concentration retrieval, the influence of NO_2 on SO_2 concentration retrieval can be ignored.

In order to study the influence of NO on the concentration retrieval of SO_2, the data collection process of the mixed gases of SO_2 and NO in the experiment is as follows. 45 ppm SO_2 and NO with different concentrations were filled into the absorption cell, and the concentration range of NO was from 40 ppm to 104 ppm at intervals of 4 ppm. The data processing process of NO and SO_2 mixed gases was similar to that of SO_2 and NO_2 mixed gases, and the data processing results are shown in Fig. 13. It can be seen from Fig. 13 that NO has hardly any influence on the eigenvalues of SO_2 concentration, so the influence of NO on the concentration retrieval of SO_2 can be ignored.

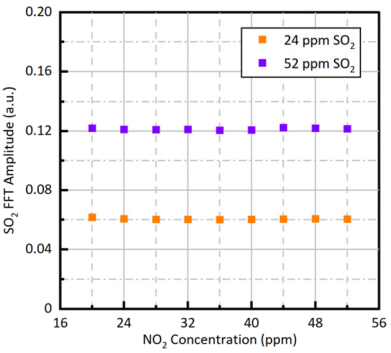

Fig. 12 Influence of NO_2 concentration change on the SO_2 FFT amplitude at 0.628 nm^{-1}.

4.2.2 NO_2 concentration retrieval. Just like the concentration retrieval process of single NO_2 gas, the wavelength range of 229.1–254.4 nm was selected as the retrieval wavelength band of NO_2 in the mixed gases, and the FFT amplitude at 0.315 nm^{-1} of the absorbance in this band was used as the eigenvalue for the concentration retrieval of NO_2 mixed with SO_2 or NO.

As shown in Fig. 1, NO_2 has a large differential absorption cross-section in this band and the spectral signal of other gases is weak, so this band has better conditions for extracting concentration eigenvalues than other bands. The experiment collected the spectral signals of different concentrations of NO_2 and SO_2 gas mixtures. The concentrations of NO_2 are 36 ppm and 52 ppm, and the concentration range of SO_2 is from 20 ppm to 52 ppm at intervals of 4 ppm. The relationship between the concentration eigenvalues of the NO_2 and SO_2 concentrations is shown in Fig. 14. As shown in Fig. 14, the

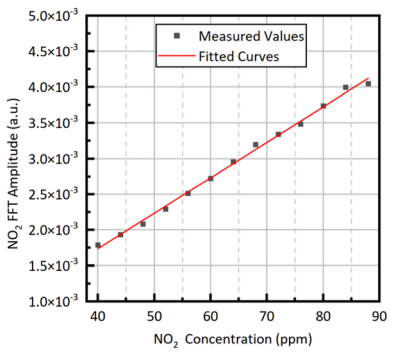

Fig. 11 Relationship between NO_2 concentration and the FFT amplitude at 0.315 nm^{-1}.

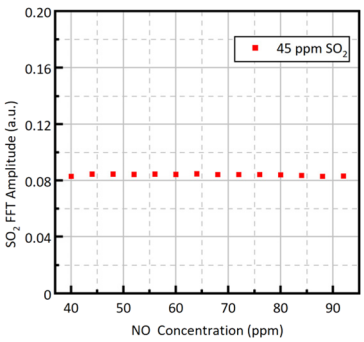

Fig. 13 Influence of NO concentration change on the SO_2 FFT amplitude at 0.628 nm^{-1}.

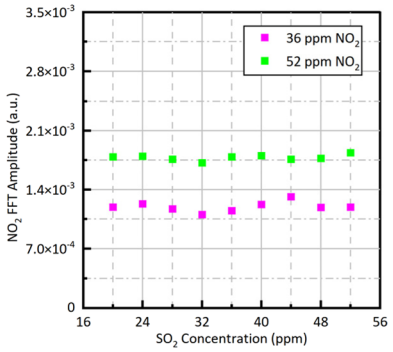

Fig. 14 Influence of SO_2 concentration change on the NO_2 FFT amplitude at 0.315 nm^{-1}.

concentration eigenvalues of NO_2 don't show significant change with the changes of SO_2 concentration. Therefore, the FFT amplitude at 0.315 nm^{-1} of the absorbance at 229.1–254.4 nm can effectively reduce the influence of SO_2 on the concentration retrieval of NO_2.

The experiment collected the spectral signals of mixtures of 50 ppm NO_2 and different concentrations of NO. The concentration range of NO is from 40 ppm to 112 ppm at intervals of 4 ppm. Just like the data processing process for single NO_2, the FFT amplitude at 0.315 nm^{-1} of the absorbance at 229.1–254.4 nm was used as the eigenvalue for NO_2 concentration retrieval. The measurement results are shown in Fig. 15 and show that the concentration retrieval eigenvalues of NO_2 don't change with the concentration change of NO. This also indicates that the FFT amplitude at 0.315 nm^{-1} of the absorbance at 229.1–254.4 nm can avoid the influence of NO on the retrieval results of NO_2 concentration.

4.2.3 NO concentration retrieval. The wavelength of 192.3 nm is still selected as the retrieval wavelength for NO concentration retrieval in mixed gases. Unlike the concentration retrieval process of SO_2 or NO_2 in mixed gases, the direct absorption method is used for the concentration retrieval of NO. Due to the absorption of SO_2 and NO_2 at 192.3 nm, it is necessary to remove the absorbances of NO_2 and SO_2 at this wavelength by post-processing. Then, the NO concentration is retrieved according to eqn (12). Due to the fact that the relationship between the absorbance at 192.3 nm and the eigenvalue of the gas concentration is a characteristic of the gas itself, it doesn't change with the change of gas concentration. Therefore, in this paper, the concentration eigenvalue of NO_2 or SO_2 is used to calibrate the absorbance of NO_2 or SO_2 at 192.3 nm.

The experiment collected 26 groups of spectral signals of SO_2 with different concentrations, ranging from 42 to 142 ppm. The relationship between the concentration eigenvalues of SO_2 and the absorbances at 192.3 nm is shown in Fig. 16. From Fig. 16, it can be seen that there is a good linear relationship between them, and the absorbance of SO_2 at 192.3 nm can be calibrated by the concentration eigenvalue of SO_2. The fitting relationship between them is shown in eqn (15), where AMP_{SO_2} is the SO_2 FFT amplitude at 0.628 nm^{-1} and $A_{192.3\_SO_2}$ is the SO_2 absorbance at 192.3 nm, and the goodness of fit between them reaches 0.9989.

$$A_{192.3\_SO_2} = 5.733 \times AMP_{SO_2} - 0.154 \quad (15)$$

The experiment collected 15 groups of spectral signals of NO_2 with different concentrations, ranging from 32 ppm to 88 ppm. Fig. 17 shows the relationship between the concentration eigenvalues of NO_2 and the absorbances of NO_2 at 192.3 nm. As shown in Fig. 17, there is a linear relationship between the concentration eigenvalues of NO_2 and the absorbances of NO_2 at 192.3 nm. The relationship between them is

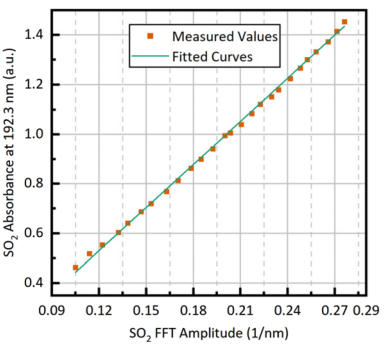

Fig. 16 Relationship between the SO_2 absorbance at 192.3 nm and SO_2 FFT amplitude at 0.628 nm^{-1}.

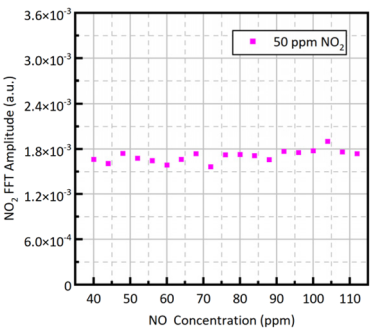

Fig. 15 Influence of NO concentration change on the NO_2 FFT amplitude at 0.315 nm^{-1}.

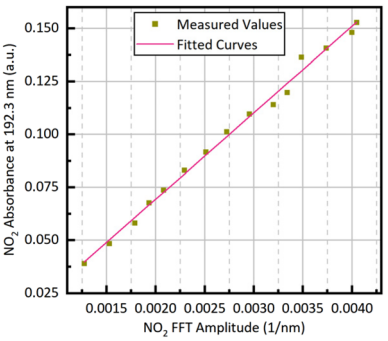

Fig. 17 Relationship between the NO_2 absorbance at 192.3 nm and NO_2 FFT amplitude at 0.315 nm^{-1}.

shown in eqn (16), where AMP_{NO_2} is the NO_2 FFT amplitude at 0.315 nm^{-1} and $A_{192.3\_NO_2}$ is the NO_2 absorbance at 192.3 nm, and the goodness of fit between them reaches 0.9941.

$$A_{192.3\_NO_2} = 40.819 \times AMP_{NO_2} - 0.012 \quad (16)$$

4.3 Retrieval method of ternary-gas

The concentration retrieval process of NO, NO_2 and SO_2 mixed gases is shown in Fig. 18. Its detailed process description is as follows.

(1) The absorbance of the mixed gases at 193–223 nm is FFT transformed, and then the SO_2 concentration in the mixed gases is calculated by the FFT amplitude at 0.628 nm^{-1} and eqn (13).

(2) The absorbance of mixed gases at 229.1–254.4 nm is FFT transformed, and then the NO_2 concentration in the mixed gases is calculated by the FTT amplitude at 0.315 nm^{-1} and eqn (14).

(3) The absorbance at 192.3 nm of the SO_2 in mixed gases is obtained by eqn (15) and the FFT amplitude at 0.628 nm^{-1} which was obtained from Step 1.

(4) The absorbance at 192.3 nm of the NO_2 in mixed gases is obtained by eqn (16) and the FFT amplitude at 0.315 nm^{-1} which was obtained from Step 2.

(5) The NO concentration in the mixed gases can be calculated by eqn (12).

4.4 Verification of the ternary-gas retrieval method

The spectral signals of gas mixtures with different concentrations of NO, NO_2, and SO_2 were collected in the experiment, and the concentrations of each component gas were retrieved according to the flowchart shown in Fig. 18. The retrieval results and measured concentrations of each component are shown in Table 1, where C_s is the setting concentration, C_d is the retrieval concentration, and $|\Delta C|$ is the absolute value of relative deviations. In Table 1, the maximum absolute values of the relative deviations for the concentration retrieval of SO_2, NO_2, and NO in ternary-gas mixtures are 3.868%, 4.740%, and 5.009%, respectively. From the data in Table 1, it can be seen that the process in Fig. 18 can perform high-precision concentration retrieval of NO, NO_2 and SO_2 mixed gases.

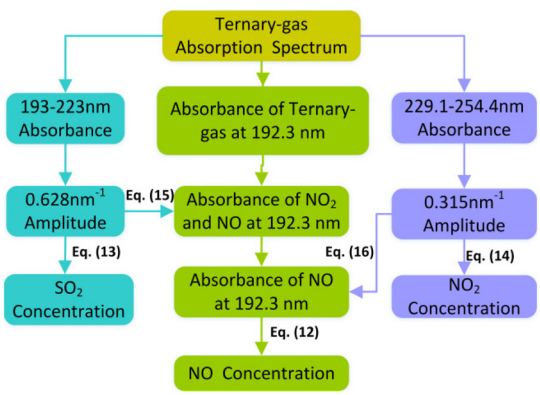

Fig. 18 Flow chart of ternary-gas concentration retrieval.

Table 1 Results of ternary-gas concentration retrieval

SO_2 (ppm)			NO_2 (ppm)			NO (ppm)		
C_s	C_d	$\|\Delta C\|$ (%)	C_s	C_d	$\|\Delta C\|$ (%)	C_s	C_d	$\|\Delta C\|$ (%)
25	25.967	3.868	28	26.673	4.739	28	27.633	1.311
28	28.110	0.393	32	31.207	2.478	26	24.813	4.565
30	29.650	1.167	35	34.061	2.683	24	22.798	5.008
35	35.312	0.891	38	36.264	4.568	20	19.058	4.710

5. Conclusions

In this paper, different wavelength bands were selected for the concentration retrieval of different gases: the wavelength range of 193–223 nm was selected for SO_2 concentration retrieval, because SO_2 has a large absorption cross-section in this band; as NO_2 has a big differential absorbance at the wavelength range of 229.1–254.4 nm, this band was selected as the concentration retrieval range of NO_2; and the wavelength of 192.3 nm was selected as the concentration retrieval wavelength of NO. The FFT amplitude method was used for the concentration retrievals of NO_2 and SO_2 and the direct absorption method was used for the concentration retrieval of NO. The spectral signals of SO_2, NO_2, and NO in mixed gases were effectively separated by selecting different wavelength bands and using different retrieval methods. The experimental results show that the concentration retrieval of ternary-gas can be achieved based on the flowchart in Fig. 18. This study makes it possible to accurately and quantitatively analyze the concentrations of SO_2, NO_2 and NO mixed gases based on ultraviolet absorption spectroscopy. These methods possess the potential to be applied to online flue detection equipment.

Author contributions

Yibiao Yang: conceptualization, methodology, software, investigation, writing-original draft. Jinhuan Li: data curation, formal analysis, writing-review. Zihui Zhang: editing and visualization, validation. Jianing Wang: resources and supervision. Guanyu Lin: project administration and funding acquisition.

Conflicts of interest

There are no conflicts to declare.

Acknowledgements

This work was supported by National Natural Science Foundation of China under Grant 62005268; Key Research and Development Program of JiLin Province under Grant 20210203174SF and 20220203195SF.

References

1 B. Peng, C. Gao, Y. Zhou and Y. Guo, *Sens. Actuators, B*, 2020, **312**, 127988.
2 J. Zou and F. Wang, *Chin. Opt. Lett.*, 2020, **18**(2), 021201.
3 S. C. Lee, B. W. Hwang, S. J. Lee, H. Y. Choi, S. Y. Kim, S. Y. Jung, D. Ragupathy, D. D. Lee and J. C. Kim, *Sens. Actuators, B*, 2011, **160**(1), 1328–1334.
4 J. Mellqvist, H. Axelsson and A. Rosen, *J. Quant. Spectrosc. Radiat. Transf.*, 1996, **56**, 225–240.
5 G. Dooly, E. Lewis, C. Fitzpatrick and P. Chambers, *IEEE Sens. J.*, 2007, **7**(5), 685–691.
6 C. Xu, H. Chen, Y. Yan and S. Wang, *Fuels*, 2015, **151**, 73–82.
7 Y. Zhou, C. Gao and Y. Guo, *J. Mater. Chem. A*, 2018, **6**, 10286–10296.
8 Emission Standard of Air Pollutants for Thermal Power Plant, State Environmental Protection Administration of China, 2011.
9 S. O. Afolaranmi, B. Ramis Ferrer and J. L. Martinez Lastra, *Int. J. Environ. Health Res.*, 2018, **28**(3), 253–279.
10 X. Ai, Y. Zhang and Z. Zhang, *Analyst*, 2022, **147**(19), 4365–4370.
11 J. Li, B. Yu and H. Fischerb, *Appl. Spectrosc.*, 2015, **69**, 496–506.
12 X. T. Lou, G. Somesfalean, Z. G. Zhang and S. Svanberg, *Appl. Phys. B*, 2009, **94**(4), 699–704.
13 M. Xu, C. Gao and Y. Guo, *Optik*, 2022, **262**, 169351.
14 B. Peng, Y. Zhou, G. Liu, Y. He, C. Gao and Y. Guo, *Spectrochim. Acta, Part A*, 2020, **233**, 118169.
15 H. S. Wang, Y. G. Zhang, S. H. Wu, X. T. Lou, Z. G. Zhang and Y. K. Qin, *Appl. Phys. B*, 2010, **100**(3), 637–641.
16 H. Keller-Rudek, G. K. Moortgat, R. Sander and R. Sörensen, *Earth Syst. Sci. Data*, 2013, **5**, 365–373.
17 A. Al-Jalal, W. Al-Basheer, K. Gasmi and M. S. Romadhon, *Measurement*, 2019, **146**, 613–617.
18 L. Li, H. Zhao, N. Ni, Y. Wang, J. Gao, Q. Gao, Y. Zhang and Y. Zhang, *Spectrochim. Acta, Part A*, 2022, **275**, 121192.
19 L. Wang, X. Deng, X. Zhang, Z. Song and Z. Zhang, *Appl. Opt.*, 2022, **61**(15), 4254–4258.
20 Y. Li, Y. Huang, Y. Shi, C. Deng, C. Hu, Y. Dong, X. Zhang and T. Wang, *IEEE Sens. J.*, 2021, **21**(16), 17889–17897.
21 H. Xiao, H.-Y. Tam, L. Dong, K. Xu, J. Zhu, P. Bo, C. Fang, G. Yongcai and G. Chao, *Optoelectronic Measurement Technology and Systems*. 2018.
22 X. Zhang, Z. Cui, Z. Cheng, Y. Li and H. Xiao, *RSC Adv.*, 2017, **7**(80), 50889–50898.
23 Y. Zhang, Y. Wang, Y. Liu, X. Dong, H. Xia, Z. Zhang and J. Li, *Spectrochim. Acta, Part A*, 2019, **210**, 120–125.
24 Y. Yang, J. Wang, Z. Zhang and G. Lin, *RSC Adv.*, 2023, **13**(28), 19149–19157.